

Estimating overlap of daily activity patterns from camera trap data

M. S. Ridout^{1*} and M. Linkie²

¹ Institute of Mathematics, Statistics and Actuarial Science,
University of Kent, Canterbury, Kent CT2 7NF, U.K.

² Durrell Institute of Conservation and Ecology,
University of Kent, Canterbury, Kent CT2 7NR, U.K.

*email: m.s.ridout@kent.ac.uk

May 9, 2008

Abstract

Data from camera traps that record the time of day at which photographs are taken are used widely to study daily activity patterns of photographed species. It is often of interest to compare activity patterns, for example between males and females of a species or between a predator and a prey species. In this article we propose that the similarity between two activity patterns may be quantified by a measure of the extent to which the patterns overlap. Several methods of estimating this overlap measure are described and their comparative performance for activity data is investigated in a simulation study. The methods are illustrated by comparing activity patterns of three sympatric felid species using data from camera traps in Kerinci Seblat National Park, Sumatra.

Keywords

circular data; clouded leopard; golden cat; kernel density estimation; overlap coefficient; Sumatran tiger; trigonometric series distribution.

1 Introduction

Tropical rain forests contain some of the highest levels of species diversity and abundance, but many tropical species are cryptic, shy and secretive, which makes them notoriously difficult to study. Consequently, these species, and their interactions with one another, remain poorly understood. This is the case especially for medium-large bodied rainforest carnivores.

Camera trap surveys provide one important source of data on these species. Typically, camera traps record the date and time at which each photograph is taken, allowing analysis of activity patterns with much improved precision over physical traps used for small mammals, which can be visited only infrequently, and typically pinpoint activity only within a range of a few hours (e.g. Rychlik, 2005). Nonetheless, camera trap times are commonly presented by grouping the capture times into hourly, two-hourly or occasionally irregular intervals (Jácomo, Silveira and Diniz-Filho, 2004). As in other contexts, it may be preferable to present kernel density estimates, for reasons discussed by Wand and Jones (1995, Section 1.2), for example.

In this paper we consider how to quantify the temporal overlap between pairs of activity patterns. Comparisons of interest might include predator and prey species (e.g. Weckel, Guiliano and Silver, 2006) or males and females of a species (e.g. Di Bitetti, Paviolo and De Angelo, 2006).

We regard the observed capture times as random samples from underlying absolutely continuous distributions and seek measures of overlap between the probability density functions (p.d.f.s) of these distributions. We focus on one particular measure of overlap, the coefficient of overlapping, and estimate this nonparametrically using kernel density estimates, following the approach of Schmid and Schmidt (2006). The key difference here is that the recorded variable, time-of-day, is a circular random variable whose underlying density may well be bimodal. The precision of the estimator of overlap is estimated by bootstrapping.

To illustrate the methodology, we investigate temporal activity pattern overlap of three sympatric carnivore species, tiger (*Panthera tigris*), clouded leopard (*Neofelis diardi*) and golden cat (*Catopuma temminckii*), from four camera trap study areas in Kerinci Seblat National Park, Sumatra. Previous studies have speculated that the clouded leopard alters its behaviour according to competition with larger carnivores and may even be less nocturnal in Borneo, where other large carnivores, such as tiger, are absent (Davis, 1962; Rabinowitz *et al.*, 1987). However, a more important potential source of interspecific competition may exist between the similar-sized clouded leopard (11-20 kg) and golden cat (9-15 kg) (Nowell and Jackson, 1996). Camera trap studies are now providing data with which these species interactions can be investigated.

The paper is organised as follows. In Section 2 we discuss briefly some measures of overlap. In Section 3 we discuss nonparametric estimation of the coefficient of overlapping, including details of the kernel density estimation procedure when the data are circular. Section 4 presents some results from a simulation study that investigates the effect of different choices of bandwidth and Section 5 presents the results of the analysis of the data from Kerinci Seblat National Park.

2 Measures of overlap

Many different measures have been suggested for quantifying the *affinity* or *overlap* of two probability density functions $f(x)$ and $g(x)$. Examples include

$$\begin{aligned}\Delta(f, g) &= \int \min \{f(x), g(x)\} dx && \text{(Weitzman, 1970),} \\ \rho(f, g) &= \int \sqrt{f(x)g(x)}dx && \text{(Matusita, 1955),} \\ \lambda(f, g) &= 2 \int f(x)g(x)dx / \left\{ \int [f(x)]^2 dx + \int [g(x)]^2 dx \right\} && \text{(Morisita, 1959).}\end{aligned}$$

The notation and attributions here follow Mulekar and Mishra (2000). Because fields of application are diverse, these measures have often been re-invented and analogous measures, with integrals replaced by sums, have also been proposed for measuring overlap of discrete distributions. In the specific context of measuring

overlap of ecological niches, these and other measures are discussed, for example, by Hurlbert (1978) and by Slobodchikoff and Schulz (1980).

Measures of overlap are often related to well-known measures of distance between densities. For example, $\Delta(f, g)$ is related to the L_1 distance between the densities,

$$\Delta(f, g) = 1 - \frac{1}{2} \int |f(x) - g(x)| dx$$

and ρ is similarly related to the Hellinger distance. A useful survey of distance measures is provided by Devroye (1987; Chapter 1), which includes, for example, a proof of LeCam's inequality

$$\Delta(f, g) \geq \frac{1}{2} \rho(f, g)^2.$$

In this paper, we focus on $\Delta(f, g)$ and write this simply as Δ unless we wish to clarify the densities involved. This measure, which is known as the *coefficient of overlapping*, has the advantage of being a natural measure of overlap that is easily interpreted geometrically. A probabilistic interpretation is that for any (Borel) subset of times A , the difference in $\Pr(A)$ for the two distributions is at most $1 - \Delta$ (Devroye, 1987, Schmid and Schmidt, 2006). For any densities $f(x)$ and $g(x)$, Δ lies in the interval $[0, 1]$, with $\Delta = 1$ if and only if the densities are identical and $\Delta = 0$ if and only if $f(x)g(x) = 0$ for all x (Clemons and Bradley, 2000). For activity patterns, $\Delta = 0$ could arise if one species was strictly diurnal and the other strictly nocturnal, for example.

Another general advantage of this measure of overlap, which follows from its relationship to L_1 distance, is that it is invariant under strictly monotonic transformations (Devroye, 1987); if X and Y are random variables with p.d.f. $f(x)$ and $g(x)$ respectively, and if ψ is a strictly monotonic function, then the overlapping coefficient of $\psi(X)$ and $\psi(Y)$ is the same as that of X and Y . Whilst this property does not appear to have direct practical relevance to camera trap data, it does form the basis of one of the alternative estimators of Δ considered in Section 3 (Schmid and Schmidt, 2006).

Finally, we note one simple property of Δ , that is a direct consequence of the fact

that L_1 distance satisfies the triangle inequality and that is relevant to the example in Section 6. Suppose that $f(x)$ and $g(x)$ are mixture densities of the form

$$f(x) = \sum_{i=1}^n w_i f_i(x) \quad \text{and} \quad g(x) = \sum_{i=1}^n w_i g_i(x),$$

where $\{f_i(x)\}$ and $\{g_i(x)\}$ are densities and $\sum_{i=1}^n w_i = 1$. Then

$$\sum_{i=1}^n w_i \Delta(f_i, g_i) < \Delta(f, g). \quad (1)$$

3 Nonparametric estimation of Δ

In the absence of any strong prior belief about the parameteric form of the underlying densities $f(x)$ and $g(x)$, it is natural to consider estimating these measures of overlap nonparametrically, by applying the measures to estimators $\widehat{f}(x)$ and $\widehat{g}(x)$ of the densities $f(x)$ and $g(x)$. This approach, with the density estimators taken to be kernel density estimators, is discussed by Ahmad (1980a), Ahmad (1980b) and Clemons and Bradley (2000) for the measures λ , ρ and Δ , respectively.

Nonparametric estimation of Δ is studied in more detail by Schmid and Schmidt (2006), who note several equivalent mathematical expressions for Δ which lead to five different estimators. They establish the consistency of these estimators under weak regularity conditions. We consider four of their estimators, excluding one (\widehat{OVL}_3 in their notation) which is not invariant to the choice of origin for circular data.

Let x_1, \dots, x_n and y_1, \dots, y_m denote the two sets of sample times. For camera trap data, the sample sizes m and n will usually differ. The four estimators that we

consider are defined as

$$\widehat{\Delta}_1 = \int_0^1 \min \left\{ \widehat{f}(t), \widehat{g}(t) \right\} dt \quad (2)$$

$$\widehat{\Delta}_2 = 1 - \frac{1}{2} \int_0^1 |\widehat{f}(t) - \widehat{g}(t)| dt \quad (3)$$

$$\widehat{\Delta}_4 = \frac{1}{2} \left(\frac{1}{n} \sum_{i=1}^n \min \left\{ 1, \frac{\widehat{g}(x_i)}{\widehat{f}(x_i)} \right\} + \frac{1}{m} \sum_{j=1}^m \min \left\{ 1, \frac{\widehat{f}(y_j)}{\widehat{g}(y_j)} \right\} \right) \quad (4)$$

$$\widehat{\Delta}_5 = \frac{1}{n} \sum_{i=1}^n I \left\{ \widehat{f}(x_i) < \widehat{g}(x_i) \right\} + \frac{1}{m} \sum_{j=1}^m I \left\{ \widehat{g}(y_j) \leq \widehat{f}(y_j) \right\}, \quad (5)$$

where $I(\cdot)$ is an indicator function and where the subscripts attached to the various estimators match those of Schmid and Schmidt (2006). The integrals in equations (2) and (3) are evaluated using the trapezoidal rule on a grid of 512 equally spaced points. In general, this results in distinct estimators which, in the simulations of Schmid and Schmidt (2006), sometimes had different properties. For circular data, however, where the density is constrained to be equal at the endpoints of the distribution, it can be shown that use of the trapezoidal rule gives identical values for $\widehat{\Delta}_1$ and $\widehat{\Delta}_2$ and we therefore have just three distinct estimators to consider.

For any of these estimators we may estimate standard errors by the bootstrap. We follow Clemons and Bradley (2000) and Schmid and Schmidt (2006) in using 200 bootstrap samples.

4 Estimating the densities $f(x)$ and $g(x)$

The estimators of Δ described in the previous section require estimators of the densities $f(x)$ and $g(x)$. In keeping with earlier work, we concentrate on kernel density estimators but, for comparison, we also consider estimating the densities within a flexible parametric framework proposed recently by Fernández-Durán (2004).

4.1 Kernel density estimation

Schmid and Schmidt (2006) use a Gaussian kernel with bandwidth h chosen by Silverman's (1986) rule, $h = 1.06\sigma n^{-1/5}$. Clemons and Bradley (2000) prefer the alternative form of this rule in which σ is replaced by $IQR/1.34$ if this is less than σ , where IQR is the interquartile range.

For circular data, we proceed analogously, using recent results of Taylor (2008). We consider estimation of $f(x)$ from the sample x_1, x_2, \dots, x_n ; estimation of $g(x)$ proceeds in the same way. The angle between an arbitrary point x in $[0, 2\pi)$, and the i th sample point is

$$a(x, x_i) = \min(|x - x_i|, 2\pi - |x - x_i|)$$

and the *angular distance* between the points is then

$$d(x, x_i) = 1 - \cos[a(x, x_i)],$$

(Jammalamadaka and SenGupta, 2001, p. 17). The kernel density estimator that we consider has the form

$$\hat{f}(x; \nu) = \frac{1}{n} \sum_{i=1}^n K_\nu [d(x, x_i)]$$

where K_ν is the p.d.f. of the von Mises distribution with mode at zero and concentration parameter ν (Jammalamadaka and SenGupta, 2001, Section 12.9).

As usual in kernel density estimation, a critical issue is the choice of the smoothing parameter, represented here by the von Mises concentration parameter ν (roughly analogous to $1/h^2$ in the case of a Gaussian kernel). Taylor (2008) shows that if the data arise from a von Mises distribution with concentration parameter κ , then the asymptotic integrated mean squared error (AMISE) is minimised by choosing

$$\nu = \left[\frac{3n\kappa^2 I_2(2\kappa)}{4\pi^{1/2} I_0(\kappa)^2} \right]^{2/5}, \quad (6)$$

where $I_r(\cdot)$ is the modified Bessel function of order r . Taylor (2008) then considers various ways of calculating a suitable robust estimate of κ to plug into equation (6)

when the underlying distribution may not be a von Mises distribution. One simple approach that generally works quite well in Taylor's simulations is to let

$$\hat{\kappa} = \max\{\hat{\kappa}_k, k = 1, \dots, K\},$$

where the estimators $\hat{\kappa}_k$ are solutions of the equations

$$A_k(\kappa) = \frac{1}{n} \sum_{i=1}^n \cos(kx_i - \hat{\mu}_k),$$

where $A_k(\kappa) = I_k(\kappa)/I_0(\kappa)$ and where $\hat{\mu}_k$ is the direction of k th sample trigonometric moment (Jammalamadaka and SenGupta, 2001, Section 1.3). If the data are from a von Mises distribution with concentration parameter κ then $\hat{\kappa}_1$ is the maximum likelihood estimate of κ and values of $\hat{\kappa}_k$ for $k > 1$ should be similar. But if the underlying distribution is not von Mises, the estimators $\hat{\kappa}_k$ are expected to differ (Taylor, 2008).

This is illustrated in Figure 1, which shows two densities, one representing a species that is predominantly diurnal and the other a species that is crepuscular, with greater activity around sunrise than around sunset. The solid lines in the plots represent the true density and the rug plot indicates a random sample of size 100 from this density that was used to calculate kernel density estimates. We set $K = 3$ and plotted kernel density estimates from choosing $\hat{\kappa} = \hat{\kappa}_1$ and $\hat{\kappa} = \max(\hat{\kappa}_1, \hat{\kappa}_2, \hat{\kappa}_3)$. In both examples, the latter choice gave $\hat{\kappa} = \hat{\kappa}_3$. For the unimodal distribution, the choice of $\hat{\kappa}$ made little difference to the resulting density estimate. For the bimodal distribution, setting $\hat{\kappa} = \hat{\kappa}_1$ gave a very poor estimate, whereas $\hat{\kappa} = \hat{\kappa}_3$ captured the main features of the bimodal distribution.

4.2 Estimation by non-negative trigonometric sums

Fernández-Durán (2004) has proposed a class of circular distributions with probability density function of the form

$$f(t) = \frac{1}{2\pi} + \frac{1}{\pi} \sum_{p=1}^P \{a_p \cos(2\pi pt) + b_p \sin(2\pi pt)\} \quad (0 \leq t \leq 1). \quad (7)$$

Somewhat complicated restrictions on the parameters $\{a_p\}$ and $\{b_p\}$ are required to ensure that the density remains non-negative. However, for a given value of P , maximum likelihood estimates of $\{a_p\}$ and $\{b_p\}$ may be calculated numerically. Our experience is that the likelihood surface often has multiple local optima and it is therefore important to run the numerical optimisation multiple times, from different starting values, to try to ensure that the global optimum has been found. As a result, fitting the distribution requires much more computation time than kernel density estimation. It is also necessary to choose an appropriate value of P . Fernández-Durán (2004) suggests choosing P to minimize the Akaike information criterion (AIC). There may be more than one local minimum of AIC as a function of P and in numerical work we have chosen the smallest local minimum. Once the densities are estimated, calculation of the various estimators of overlap proceeds as in Section 3; examples are provided in Section 6.

5 Simulation study

Figure 2 shows twelve hypothetical activity patterns chosen to represent types of activity likely to be encountered in practice. Those in the first column represent species that are active primarily during the day; they differ in the strength of the day time peak and the extent to which a reduced level of activity occurs during the night. The distributions in the second column of Figure 2 are identical to those in the first column, except that times have been shifted by twelve hours. Thus the roles of day and night are interchanged. The final column shows patterns for crepuscular species, with two peaks of activity; they differ in the strength and symmetry of the peaks. The 66 distinct pairs that can be formed from these distributions have overlap coefficients ranging from 0.015 to 0.862.

We conducted a simulation study to investigate the performance of the estimators $\widehat{\Delta}_1$, $\widehat{\Delta}_4$ and $\widehat{\Delta}_5$ when $f(x)$ and $g(x)$ were estimated by kernel density estimation. The ‘optimal’ value of the concentration parameter of the von Mises kernel, ν_{opt} , was calculated from equation (6), with $\hat{\kappa} = \max(\hat{\kappa}_1, \hat{\kappa}_2, \hat{\kappa}_3)$ substituted for κ . One

objective of the simulations was to investigate the effect of under- or over-smoothing on the resulting estimators of overlap and we therefore set the concentration parameter of the kernel to be $c\nu_{opt}$ for various values of c . Note that because ν is a concentration parameter, $c < 1$ represents over-smoothing and $c > 1$ represents under-smoothing, relative to the use of ν_{opt} .

For each of the 66 pairs of distributions, we investigated the effect of sample size ($n = m = 25, 50, 100$ or 200) and the choice of c ($= 0.1, 0.25, 0.5, 0.75, 1, 1.25, 1.5, 2$ or 4) on the bias and precision of the resulting estimators of overlap. We ran 100 simulations for each combination of factors. Comparable simulations with $f(x)$ and $g(x)$ estimated by trigonometric sum distributions were not run because they would have required a huge amount of computer time.

Each set of 100 simulations was summarised by the bias, standard deviation and root mean square error (RMSE) of the 100 estimates. Figure 3 shows boxplots of the RMSE across the 66 pairs of distributions. Often, the best distribution of RMSE values occurs for values of c other than $c = 1$ but the patterns differ markedly. For $\widehat{\Delta}_1$ and $\widehat{\Delta}_4$, the optimal choice of c increases with sample size, whereas for $\widehat{\Delta}_5$ it is consistently around $c = 0.25$.

Figure 4 shows that the patterns arise predominantly due to changing bias, with the standard deviation being relatively insensitive to the choice of c . When $c < 1$ the data are over-smoothed and in the limit as $c \rightarrow 0$, the kernel density estimates will approach uniform distributions, with $\Delta = 1$. Conversely, when c is large the kernel estimates are concentrated around the individual data points, resulting in underestimation of Δ . Consequently, we anticipate that the bias will be a decreasing function of c , as is seen in Figure 4. However, the magnitude and rate of decline of the bias depend on the estimator.

Figure 5 compares the estimators for fixed values of $c = 1.25$ for $\widehat{\Delta}_1$, $c = 1.0$ for $\widehat{\Delta}_4$ and $c = 0.25$ for $\widehat{\Delta}_5$. These choices of c perform reasonably well across the range of sample sizes considered in the simulations. The left hand panels of Figure 5 show

that for small sample sizes $\hat{\Delta}_1$ is generally preferable to $\hat{\Delta}_4$, in terms of RMSE, whereas the converse is true for large sample sizes. The central and right hand panels of Figure shows that, for each sample size, the better of these two estimators generally outperforms $\hat{\Delta}_5$.

6 Application to felid species in Kerinci Seblat National Park

The methods described above were applied to camera trap records from four study areas located in and around the 13,300km² Kerinci Seblat National Park. Across the four areas, data were recorded from 138 camera trap placements over a total of 8984 trap days. Photographs that were recorded within thirty minutes of a previous photograph at the same site were excluded from the data set because of concerns about lack of independence.

A previous analysis of some of the data from these traps (Linkie et al., 2008) estimated overlap of the activity pattern of the Sumatran tiger with activity patterns of four ungulate species considered to be tiger prey using the estimator $\hat{\Delta}_2$ (equivalent to $\hat{\Delta}_1$), though based on a different method of kernel density estimation to that described above. Here we apply the methods described in this paper to estimate activity overlap of the Sumatran tiger and two other felid species, the Asian golden cat and the clouded leopard.

Table 1 shows the number of records of each species in each study area. We begin by considering the combined data from all four study areas. Figure 6 shows kernel density estimates with $c = 1.25$, $c = 1.0$ and $c = 0.25$ and estimated trigonometric sum densities, obtained by minimising AIC, as described in Section 4.2, which gave $P = 2$ for tiger and clouded leopard and $P = 1$ for golden cat. Kernel density estimates with $c = 1.25$ or $c = 1$ are quite similar to the estimated trigonometric sum densities, but compared to these the kernel density estimate with $c = 0.25$ appears substantially undersmoothed.

Based on the results of the previous Section, we used the kernel density estimates with $c = 1.25$, $c = 1.0$ and $c = 0.25$ to calculate the estimators $\widehat{\Delta}_1$, $\widehat{\Delta}_4$ and $\widehat{\Delta}_5$, respectively. We also calculated these estimators using the trigonometric sum estimators of density. The results, shown in Table 2, indicate a high degree of overlap between tiger and golden cat and, to a lesser extent between tiger and clouded leopard, but a considerably lower level of overlap between golden cat and clouded leopard. For the relatively large sample sizes involved here, the simulation results of the previous Section suggest that $\widehat{\Delta}_4$ may be the most reliable estimator.

Whilst these analyses are useful for illustrating the methodology, they are potentially misleading, because the distributions of times appear to differ between areas, based, for example, on the test using circular ranks given in Section 5.3.6 of Fisher (1993). In particular, for clouded leopards, there is a marked difference between areas 2 and 4, where the animal appears predominantly nocturnal, and sites 1 and 3, where there are several day time observations.

Table 3 therefore provides estimates of overlap for each site separately. Because sample sizes at individual sites are often small (Table 1), we use the estimator $\widehat{\Delta}_1$, with $c = 1.25$. For tiger and golden cat, the estimates for areas 2, 3 and 4 are all similar, but the estimate for area 1 is much smaller. However, this latter estimate is based on very small samples at both sites, as reflected by its larger standard error. When comparing clouded leopard with either tiger or golden cat, the differences between areas in the capture times of clouded leopards are now reflected in the estimates of overlap, which are lower for areas 2 and 4.

The inequality (1) involving mixture distributions at the end of Section 2 implies that the values of overlap obtained for the data pooled across areas will exceed the average value for the separate areas. The numerical results in Table 3 show that the effect is quite substantial, so that pooling the data across sites substantially overestimates the extent of overlap within areas.

7 Discussion

Our main ecological objective of this paper is to advocate the use of kernel density estimation of activity patterns, particularly as a basis for measuring activity overlap. The measure of overlap that we have used has several attractive statistical properties, as outlined in Section 2. However, alternative measures, for example focusing on the degree of synchrony of peaks of activity, may also be of ecological interest.

In a broad sense, the overlap results are as one might anticipate based on the relative sizes of the species. The lowest overlap values were those between the similarly sized clouded leopard and golden cat. The much larger tiger (50–70 kg) is likely to specialise on prey of different species, body size and age-sex class (Karanth and Sunquist, 1995), limiting the need for temporal avoidance. Although golden cat and clouded leopard are of similar size, the clouded leopard has, proportionately, the longest canines amongst extant felids, and this morphological differentiation would enable it to kill larger prey than golden cat.

The recent development of an analogue for circular data of Silverman’s bandwidth rule (Taylor, 2008) allows the procedures of Schmid and Schmidt (2006) to be translated directly to circular data. However, we also investigated the effect of systematically under- or over-smoothing relative to this bandwidth and found, in particular, that for the estimator $\widehat{\Delta}_5$ it was better to over-smooth ($c < 1$). It would be interesting to investigate whether a similar effect occurs for linear data.

Our simulations suggested that it was generally best to use $\widehat{\Delta}_1$ for small sample sizes and $\widehat{\Delta}_4$ for large sample sizes. This differs somewhat from the conclusion of Schmid and Schmidt who recommended $\widehat{\Delta}_5$ on the basis of its small bias, except when the true overlap was close to one, where $\widehat{\Delta}_2$ (equivalent to $\widehat{\Delta}_1$ for circular data) was preferred. However, in their studies, as in ours, there is no uniformly best estimator. Our recommendations are intended to apply to the sorts of activity pattern that are likely to be observed in practice.

An alternative to kernel density estimation is to fit parametric distributions. Here we have explored the use of trigonometric sum distributions (Fernández-Durán, 2004), which gave similar results to the kernel density based estimates in our examples. Directional log-spline distributions (Ferreira, Juárez and Steel, 2008) might provide a useful alternative if more flexibility is required in the shape of the activity pattern.

Acknowledgements

We are grateful to the US Fish and Wildlife Service, 21st Century Tiger, Rufford Small Grants and the Peoples Trust for Endangered Species for funding this work. We are grateful to Ir. Soewartono, Dr Sugardjito and the Department of Forestry and Nature Protection for assisting us in our Indonesian work and to Yoan Dinata, Agung Nugroho and Iding Achmad Hadir for their help with the data collection. We also thank Juan Fernández-Durán for helpful discussion of trigonometric series distributions and Miguel Juárez for providing the software for fitting directional log-spline distributions.

References

- Ahmad, I.A. (1980a). Nonparametric estimation of an affinity measure between two absolutely continuous distributions with hypothesis testing applications. *Annals of the Institute of Statistical Mathematics*, **32**, 223–240.
- Ahmad, I.A. (1980b). Nonparametric estimation of Matusita's measure of affinity between absolutely continuous distributions. *Annals of the Institute of Statistical Mathematics*, **32**, 241–245.
- Clemons, T.E. and Bradley, E. L. (2000) A nonparametric measure of the overlapping coefficient. *Computational Statistics and Data Analysis*, **34**, 51–61. (Erratum: **36**, 243).
- Davis, D.D. (1962) Mammals of the lowland rain-forest of North Borneo. *Bulletin of the Singapore Natural History Museum*, **31**, 1–129.
- Devroye, L. (1987) *A Course in Density Estimation*. Boston: Birkhäuser.
- Di Bitetti, M.S., Paviolo, A. and De Angelo, C. (2006) Density, habitat use and activity patterns of ocelots (*Leopardus pardalis*) in the Atlantic Forest of Misiones, Argentina. *Journal of Zoology*, **270**, 153–163.
- Fernández-Durán, J.J. (2004) Circular distributions based on nonnegative trigonometric sums. *Biometrics*, **60**, 499–503.

- Ferreira, J.T.A.S., Juárez, M.A. and Steel, M.F. (2008) Directional log-spline distributions. *Bayesian Analysis*, **3**, 1–19.
- Fisher, N.I. (1993) *Statistical Analysis of Circular Data*. Cambridge: Cambridge University Press.
- Hurlbert, S.H. (1978) The measurement of niche overlap and some relatives. *Ecology*, **59**, 67–77.
- Jácomo, A.T.A., Silveira, L., Diniz-Filho, J.A.F. (2004) Niche separation between the maned wolf (*Chrysocyon brachyurus*), the crab-eating fox (*Dusicyon thous*) and the hoary fox (*Dusicyon vetulus*) in central Brazil. *Journal of Zoology*, **262**, 99–106.
- Jammalamadaka, S. and SenGupta, A. (2001) *Topics in Circular Statistics*. Singapore: World Scientific.
- Karranthy, K.U. and Sunquist, M.E. (1995) Prey selection by tiger, leopard and dhole in tropical forests. *Journal of Animal Ecology*, **64**, 439–450.
- Linkie, M., Borysiewicz, R.S., Dinata, Y., Nugroho, A., Achmad Hadir, I., Ridout, M.S., Leader-Williams, N. and Morgan, B.J.T. (2008) Predicting the spatio-temporal patterns of tiger and their prey across a primary-disturbed forest landscape in Sumatra. *Submitted for publication*.
- Matusita, K. (1955) Decision rules, based on the distance, for problems of fit, two samples, and estimation. *Annals of Mathematical Statistics*, **26**, 631–640.
- Morisita, M. (1959) Measuring interspecific association and similarity between communities. *Memoirs of the Faculty of Science of Kyushu University, Series E, Biology*, **3**, 65–80.
- Mulekar, M.S. and Mishra S.N. (2000) Confidence interval estimation of overlap: equal means case. *Computational Statistics and Data Analysis*, **34**, 121–137.
- Nowell, K. and Jackson, P. (1996) *Wild Cats – Status Survey and Conservation Action Plan*. Gland, Switzerland: IUCN.
- Rabinowitz, A.R., Andau, P. and Chai, P.P.K. (1987) The clouded leopard in Malaysian Borneo. *Oryx*, **21**, 107–111.
- Rychlik, L. (2005) Overlap of temporal niches among four sympatric species of shrews. *Acta Theriologica*, **50**, 175–188.
- Schmid, F. and Schmidt, A. (2006) Nonparametric estimation of the coefficient of overlapping — theory and empirical application. *Computational Statistics and*

Data Analysis, **50**, 1583–1596.

Silverman, B. (1986) *Density Estimation for Statistics and Data Analysis*. New York: Chapman and Hall.

Slobodchikoff, C.N. and Schulz, W.C. (1980) Measures of niche overlap. *Ecology*, **61**, 1051-1055.

Taylor, C.C. (2008) Automatic bandwidth selection for circular density estimation. *Computational Statistics and Data Analysis*, **52**, 3493–3500.

Wand, M.P. and Jones, M.C. (2005) *Kernel Smoothing* London: Chapman and Hall.

Weckel, M., Giuliano, W. and Silver, S. (2006) Jaguar (*Panthera onca*), feeding ecology: distribution of predator and prey through time and space. *Journal of Zoology*, **270**, 25–30.

Weitzman, M.S. (1970) Measure of the overlap of income distribution of white and Negro families in the United States. *Technical Report No. 22*, U.S. Department of Commerce, Bureau of the Census, Washington, DC.

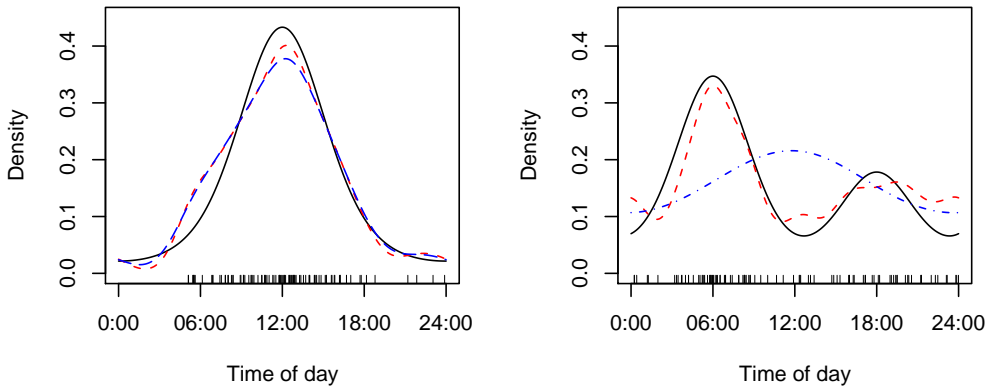


Figure 1. Illustration of the choice of smoothing parameter for kernel density estimation. The density on the left is a von Mises distribution with concentration parameter $\kappa = 1.5$. The density on the right is a mixture of two von Mises distributions, both with concentration parameter $\kappa = 2$, in proportions 0.75:0.25. The rug plot shows a random sample of 100 from each density. Dotted-dashed lines show kernel density estimates with $\hat{\kappa} = \hat{\kappa}_1$ and dashed lines show kernel density estimates with $\hat{\kappa} = \max(\hat{\kappa}_1, \hat{\kappa}_2, \hat{\kappa}_3)$.

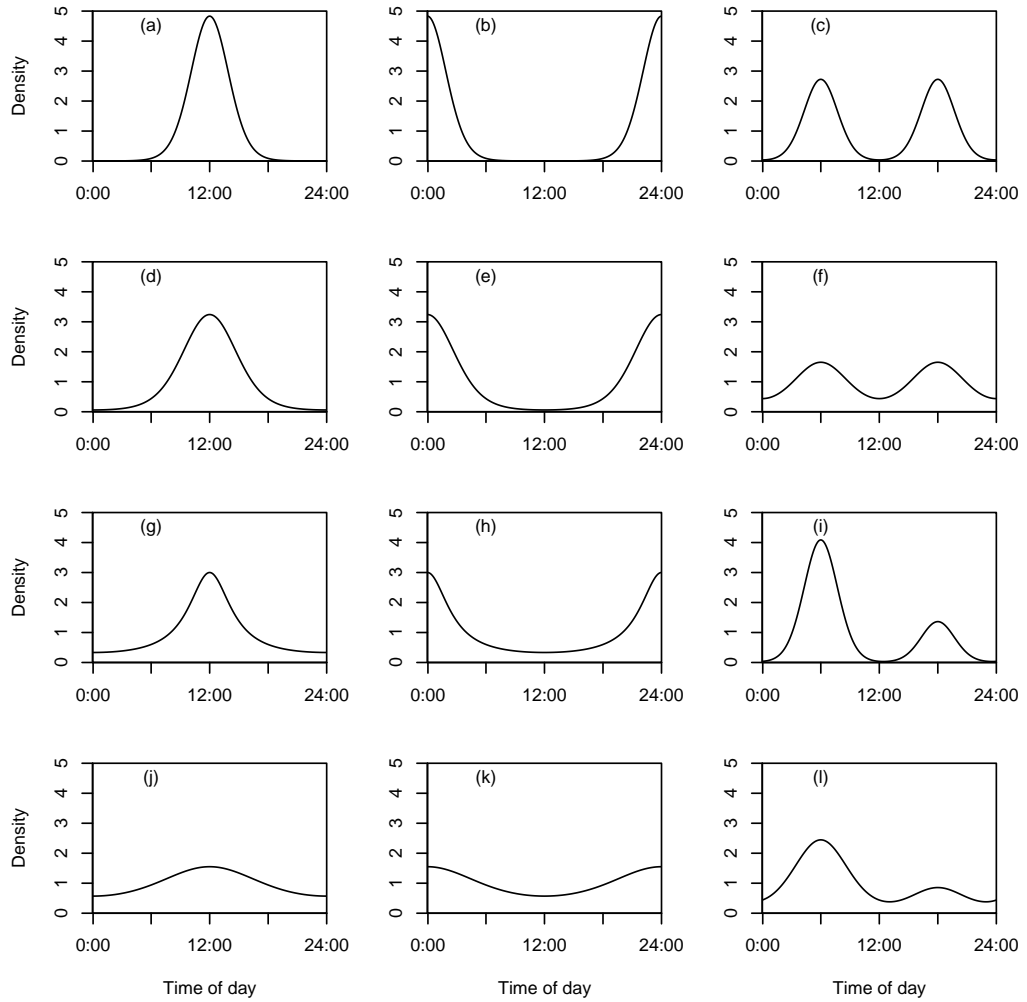


Figure 2. Twelve hypothetical activity patterns. Figures (a), (b), (d), (e), (j) and (k) are von Mises distributions; figures (c), (f), (i) and (l) are mixtures of two von Mises distributions; figures (g) and (h) are wrapped Cauchy distributions.

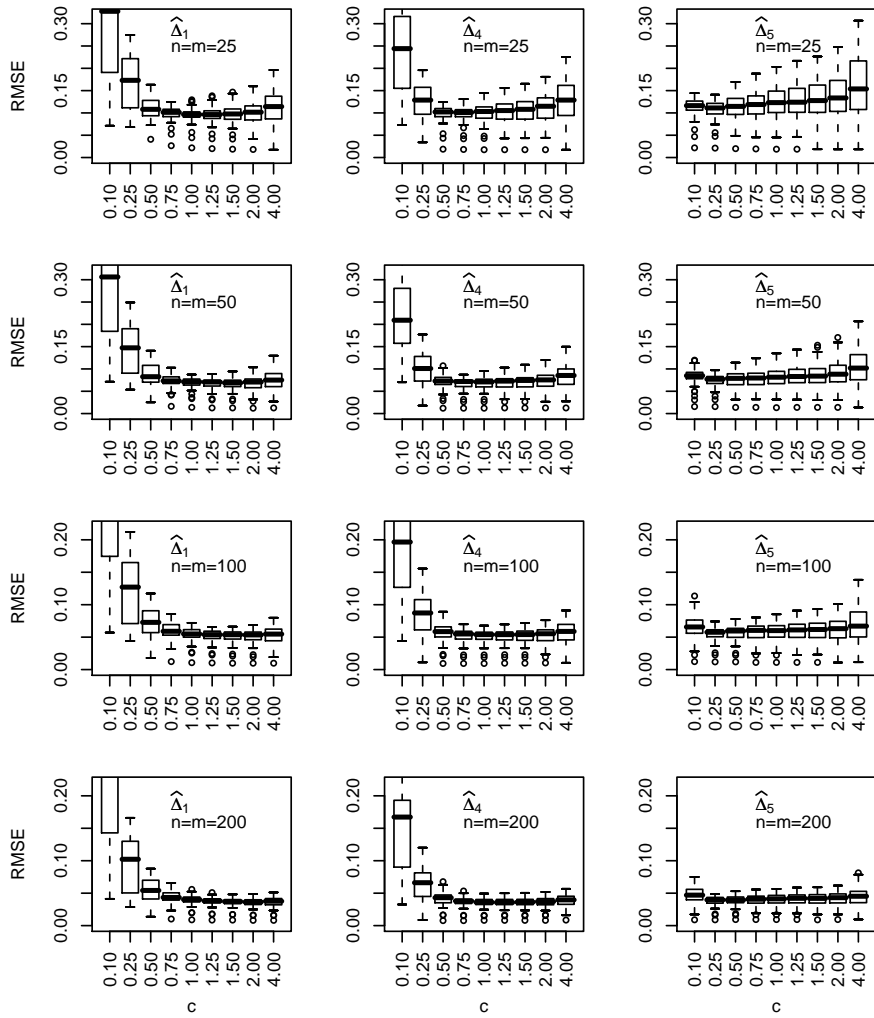


Figure 3. Boxplots of the root mean squared error (RMSE) of estimated overlap for simulated data with sample sizes $n = m = 25, 50, 100$ or 200 . Each boxplot summarises the RMSE of one of the three estimators of overlap for the 66 pairs of activity patterns. The horizontal axis shows the value of c used in determining the concentration parameter for kernel density estimation (see text). Note that the horizontal axis is not linear and that the scaling of the vertical axis differs between rows.

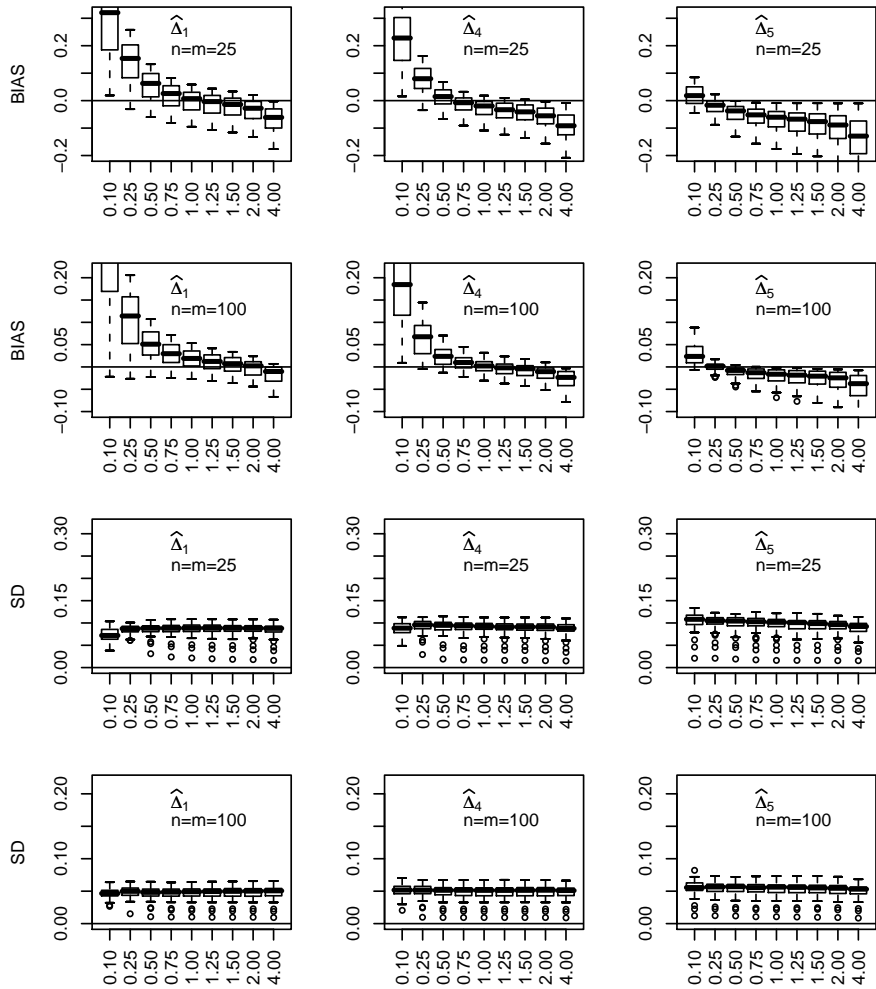


Figure 4. Boxplots of the bias and standard deviation of estimated overlap for simulated data with sample sizes $n = m = 25$ and $n = m = 100$. Each boxplot summarises the bias or standard deviation of one of the three estimators of overlap for the 66 pairs of activity patterns. The horizontal axis shows the value of c used in determining the concentration parameter for kernel density estimation (see text). Note that the horizontal axis is not linear and that the scaling of the vertical axis differs between rows.

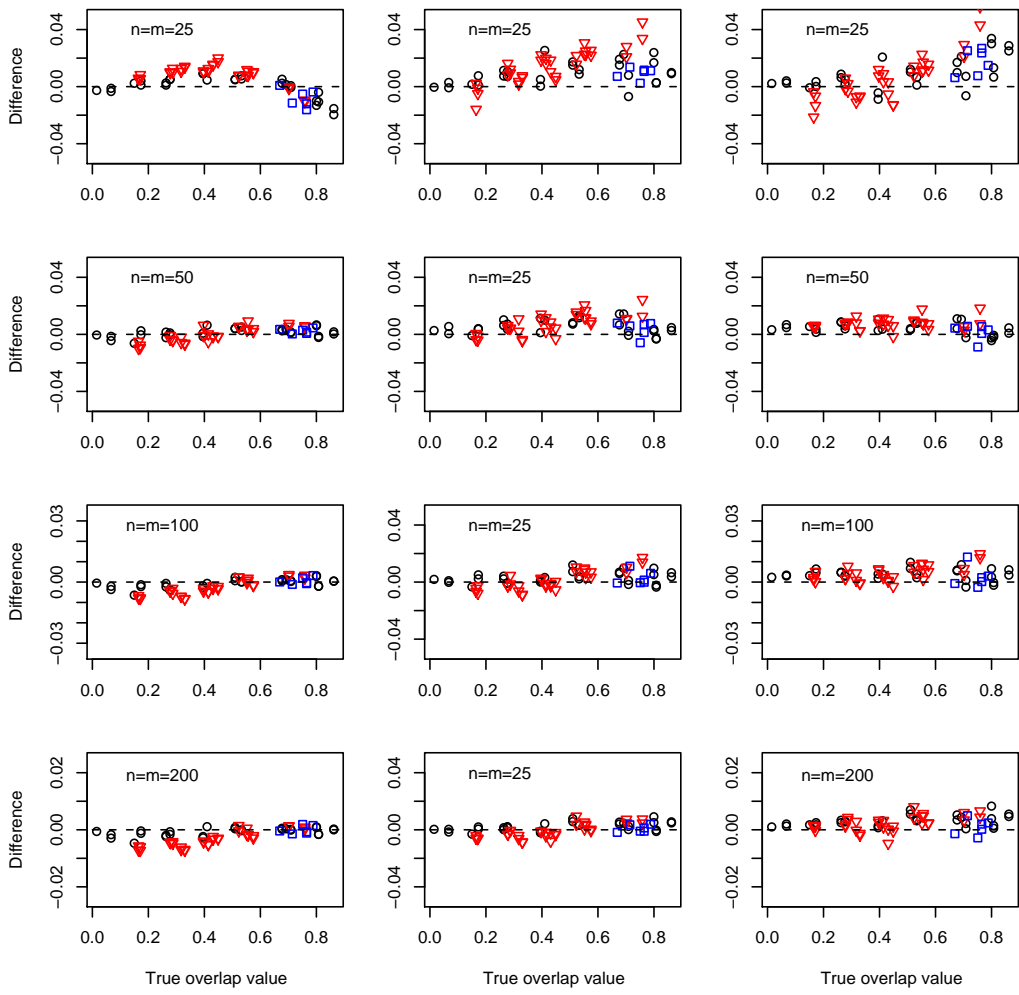


Figure 5. Differences in root mean square error (RMSE) values between estimators. The left hand column shows $\text{RMSE}(\widehat{\Delta}_4) - \text{RMSE}(\widehat{\Delta}_1)$, the middle column shows $\text{RMSE}(\widehat{\Delta}_5) - \text{RMSE}(\widehat{\Delta}_1)$, and the right hand column shows $\text{RMSE}(\widehat{\Delta}_5) - \text{RMSE}(\widehat{\Delta}_4)$. Different rows show different sample sizes, as indicated on the graphs. We set $c = 1.25$ for calculating $\widehat{\Delta}_1$, $c = 1.0$ for calculating $\widehat{\Delta}_4$ and $c = 0.25$ for calculating $\widehat{\Delta}_5$. Different symbols in the plots indicate different types of activity pattern for which the overlap was estimated; either both distributions were unimodal (circle), both were bimodal (square) or one was unimodal and the other was bimodal (triangle).

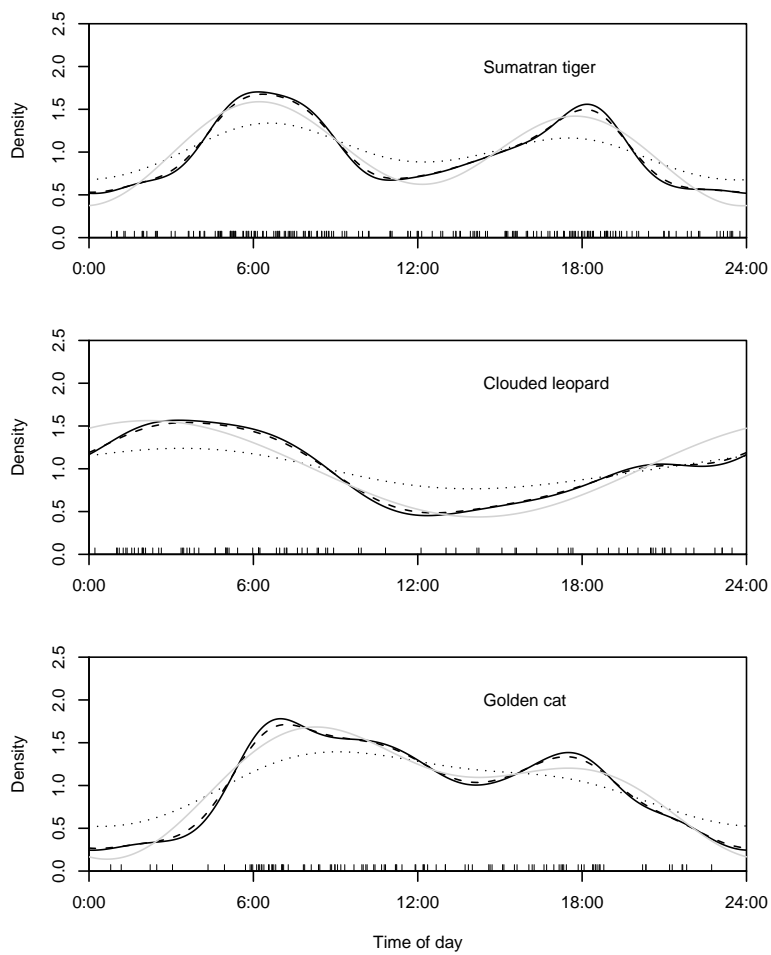


Figure 6. Estimated activity patterns for three felid species. Kernel density estimates are shown with $c = 1.25$ (solid line), $c = 1.0$ (dashed line) and $c = 0.25$ (dotted line). The light grey line is the the estimated trigonometric series density. The short vertical lines at the bottom of the plot indicate the times of day at which the species were photographed.

Table 1. Numbers of camera trap records of the three species at each site.

Species	Site				Total
	1	2	3	4	
Sumatran tiger	15	83	52	51	201
Asian golden cat	14	26	38	26	104
Clouded leopard	27	10	17	32	86

Table 2. Three estimators of overlap for the felid species. The underlying activity densities were estimated either by kernel density estimation (with $c = 1.25$ for $\hat{\Delta}_1$, $c = 1.0$ for $\hat{\Delta}_4$ and $c = 0.25$ for $\hat{\Delta}_5$) or as trigonometric series densities.

Species	Density estimator	Overlap estimator		
		$\hat{\Delta}_1$	$\hat{\Delta}_4$	$\hat{\Delta}_5$
Tiger and golden cat	Kernel density	0.859	0.865	0.889
Tiger and golden cat	Trigonometric series	0.848	0.853	0.892
Tiger and clouded leopard	Kernel density	0.794	0.780	0.754
Tiger and clouded leopard	Trigonometric series	0.761	0.774	0.749
Clouded leopard and golden cat	Kernel density	0.673	0.675	0.609
Clouded leopard and golden cat	Trigonometric series	0.653	0.665	0.617

Table 3. Estimates of overlap within each study area. The estimator used was $\hat{\Delta}_1$, with $c = 1.25$. Values in brackets are bootstrap standard errors.

Species	Area				
	1	2	3	4	All areas
Tiger and golden cat	0.56 (0.106)	0.81 (0.073)	0.81 (0.067)	0.78 (0.065)	0.86 (0.037)
Tiger and clouded leopard	0.64 (0.097)	0.58 (0.097)	0.71 (0.078)	0.47 (0.068)	0.79 (0.047)
Golden cat and clouded leopard	0.58 (0.085)	0.50 (0.103)	0.68 (0.095)	0.41 (0.083)	0.67 (0.055)